Research Square

Preprints are preliminary reports that have not undergone peer review.
They should not be considered conclusive, used to inform clinical practice,
or referenced by the media as validated information.

Multimodal Plasma Proteomic and T1-Radiomic Correlates of Memory Impairment in Biomarker-Defined Amyloid- Positive Late-Life Depression

Danyan Xu
The Affiliated Brain Hospital of Guangzhou Medical University
Pengbo Gao
The Affiliated Brain Hospital of Guangzhou Medical University
Weilin Wang
The Affiliated Brain Hospital of Guangzhou Medical University
Huanmin Liu
The Affiliated Brain Hospital of Guangzhou Medical University
Wei He
The Affiliated Brain Hospital of Guangzhou Medical University
Ting Su
The Affiliated Brain Hospital of Guangzhou Medical University
Youxuan Zheng
The Affiliated Brain Hospital of Guangzhou Medical University
Zhen Peng
The Affiliated Brain Hospital of Guangzhou Medical University
Haoye Tan
The Affiliated Brain Hospital of Guangzhou Medical University
Mingfeng Yang
The Affiliated Brain Hospital of Guangzhou Medical University
Qiang Wang
The Affiliated Brain Hospital of Guangzhou Medical University
Zhidai Xiao
The Affiliated Brain Hospital of Guangzhou Medical University
Ben Chen
The Affiliated Brain Hospital of Guangzhou Medical University
Xiaomei Zhong
The Affiliated Brain Hospital of Guangzhou Medical University
Yuping Ning
ningjeny@126.com

The Affiliated Brain Hospital of Guangzhou Medical University

Research Article

Keywords: Late-life depression, Amyloid pathology, Plasma proteomics, Radiomics, Neuroinflammation

Posted Date: November 18th, 2026

DOI: https://doi.org/10.21203/rs.3.rs-10672734/v1

License: This work is licensed under a Creative Commons Attribution 4.0 International License.
Read Full License

Additional Declarations: No competing interests reported.

Multimodal Plasma Proteomic and T1-Radiomic Correlates of Memory Impairment in Biomarker-Defined Amyloid-Positive Late-Life Depression

Danyan Xu[1#], Pengbo Gao [2,1#], Weilin Wang[1#], Huanmin Liu[1], Wei He[1], Ting Su[1], Youxuan Zheng[1], Zhen Peng[1], Haoye Tan[1], Mingfeng Yang[1], Qiang Wang[1], Zhidai Xiao[1], Ben Chen[1]*, Xiaomei Zhong[1]*, Yuping Ning [1, 3, 4, 5]*

Affiliations:

[1] Geriatric Neuroscience Center, The Affiliated Brain Hospital, Guangzhou Medical University, Guangzhou, Guangdong Province, China, 0086-510370.

[2] Brain Function Examination Center, The Affiliated Brain Hospital, Guangzhou Medical University, Guangzhou, Guangdong Province, China.

[3] Southern Medical University, Guangzhou, Guangdong Province, China, 0086-510515.

[4] Guangdong Engineering Technology Research Center for Translational Medicine of Mental Disorders, Guangzhou, Guangdong Province, China, 0086-510370.

[5] Key Laboratory of Neurogenetics and Channelopathies of Guangdong Province and the Ministry of Education of China, Guangzhou Medical University, Guangzhou, Guangdong Province, China, 510000.

[#] Danyan Xu, Pengbo Gao and Weilin Wang contributed equally to the work.

*** Corresponding authors' information:**

Ben Chen, Geriatric Neuroscience Center, The Affiliated Brain Hospital of Guangzhou Medical University, Guangzhou, Guangdong Province, China, email addresses: chenbenpielo@sina.com, Telephone: +86-020-81268181, Fax: 020-81891351 Postal: 0086-510370.

Xiaomei Zhong, Geriatric Neuroscience Center, The Affiliated Brain Hospital of Guangzhou Medical University, Guangzhou, Guangdong Province, China, email addresses: lovlaugh@163.com, Telephone: +86-020-81268181, Fax: 020-81891351 Postal: 0086-510370.

Yuping Ning, Geriatric Neuroscience Center, The Affiliated Brain Hospital, Guangzhou Medical University, Guangzhou, Guangdong Province, China, email addresses: ningjeny@126.com, Telephone: +86-020-81268181, Fax: 020-81891351 Postal: 0086-510370.

34 Main Figures: 5

35 Main Tables: 1

36

Abstract

Background: Late-life depression (LLD) is associated with an increased risk of dementia and a biologically defined subgroup exhibits amyloid pathology associated with Alzheimer's disease (AD). However, the molecular and neuroanatomical characteristics of this subgroup remain incompletely understood. Investigating the relationships among plasma proteomic profiles, T1-derived radiomic features, and cognition may help characterize biological heterogeneity at the intersection of LLD and the AD continuum.

Methods: This integrative proteomics–radiomics study included 116 LLD patients, whose AD biomarker status was defined using Core 1 biomarkers according to the 2024 Alzheimer's Association revised criteria. A machine learning–derived radiomic signature distinguishing biomarker-defined amyloid-positive from amyloid-negative LLD was constructed. The key plasma proteomic module was identified using weighted gene co-expression network analysis, and its mechanistic role was evaluated using mediation analysis.

Results: The radiomic score (RadScore) discriminated biomarker-defined amyloid-positive LLD in a held-out internal test subset (AUC=0.788), with influential features from the paracentral lobule and precuneus. It correlated with a neutrophil activation–enriched

module ($r=-0.49$, $p<0.001$). The cross-sectional indirect-effect analysis indicated that the RadScore accounted for 52.5% of the modeled association with memory performance.

Conclusions: In biomarker-defined amyloid-positive LLD, T1-derived radiomic features were associated with a plasma protein module enriched for innate immune and neutrophil-related annotations and with memory performance. These cross-modal associations require independent longitudinal validation.

Key Words

Late-life depression; Amyloid pathology; Plasma proteomics; Radiomics; Neuroinflammation.

1. Introduction

Late-life depression (LLD) may precede cognitive decline[1],and is associated with a 2- to 5-fold increased risk of developing dementia[2]. The subset of these patients biologically overlaps with Alzheimer's disease (AD), harboring amyloid-beta (Aβ) pathology even before the onset of profound cognitive decline[3]. However, while the biological overlap is established, the biological relationships linking systemic abnormalities, regional brain imaging features, and cognition remain incompletely understood.

Peripheral immune dysregulation may contribute to the pathophysiology of both LLD and AD[4, 5].Plasma proteomic studies have identified coordinated alterations in immune-inflammatory and related biological pathways in both conditions[6], supporting the use of proteomics to characterize systemic immune dysregulation beyond individual inflammatory markers. Importantly, circulating immunological markers have also been associated with reduced gray matter volume and greater white matter hyperintensity burden in LLD[7], while plasma proteomic signatures have been linked to distinct patterns of brain atrophy in AD[8]. These findings suggest that systemic immune dysregulation may be reflected in subtle and spatially distributed alterations in brain tissue.

However, these subtle and spatially distributed tissue-level alterations may not be adequately captured by conventional visual inspection or standard volumetric magnetic resonance imaging (MRI)[9]. In this context, radiomics provides a high-throughput

approach for extracting high-dimensional quantitative features that characterize image intensity, texture, and spatial patterns[10]. Unlike traditional volumetry, T1-weighted radiomics may reveal subtle tissue heterogeneity that is not reflected by regional volume alone[11]. Accordingly, T1-weighted radiomics may provide a noninvasive approach for investigating subtle tissue-level heterogeneity associated with systemic immune dysregulation in LLD.

In this study, we aimed to characterize cross-modal relationships among plasma proteomics, T1 radiomics, and cognition in LLD patients classified by biomarker-defined amyloid status. Specifically, we sought to: (1) Develop an radiomic model associated with biomarker-defined Aβ positivity; (2) Identify peripheral protein modules that correlate with this central imaging phenotype; and (3) Explore whether the RadScore statistically accounts for part of the association between a plasma protein module and domain-specific cognitive performance. This study provides an exploratory multimodal framework for characterizing biological heterogeneity in amyloid-positive LLD and for generating hypotheses for longitudinal validation.

2. Methods

2.1. Participants and Study Design

This cross-sectional study consecutively enrolled 116 patients with LLD from the outpatient clinic of the Affiliated Brain Hospital of Guangzhou Medical University and community settings across Guangzhou, China. All participants underwent comprehensive

psychiatric evaluation by experienced psychiatrists. Eligibility criteria included: age ≥ 55 years; a diagnosis of major depressive disorder according to the Diagnostic and Statistical Manual of Mental Disorders, Fifth Edition (DSM-5) ascertained using the Structured Clinical Interview for DSM-5 Disorders, with at least one depressive episode occurring after age 55; and a current 17-item Hamilton Depression Rating Scale score below 17, indicating clinical remission or partial remission; and a complete neurological physical examination to rule out cerebrovascular events. Participants were excluded if they had any comorbid DSM-5 psychiatric disorder, hypothyroidism, major systemic illness (cardiac, hepatic, or renal dysfunction), neurological conditions (central nervous system infection, stroke, traumatic brain injury, intracranial neoplasm, or epilepsy), uncorrectable visual impairment, claustrophobia, or non-right-handedness. Biomarker stratification was aligned with the Core 1 biomarker framework outlined in the 2024 revised diagnostic criteria for Alzheimer's disease[12], using a previously validated classification approach[13]. Participants were classified as amyloid-positive (LLD Aβ+) or amyloid-negative (LLD Aβ−). The complete study workflow is detailed in **Figure 1**.

2.2. Clinical and Neuropsychological Assessments

All participants underwent a standardized battery of clinical and neuropsychological assessments administered by trained professionals. Depressive symptom severity was

evaluated using the 17-item Hamilton Depression Rating Scale (HAMD-17). Global cognitive function was screened using the Mini-Mental State Examination (MMSE) and Clinical Dementia Rating Scale (CDR). Domain-specific cognitive assessments encompassed: (1) memory, evaluated via the Auditory Verbal Learning Test (AVLT), including AVLT immediate recall, AVLT short-term delayed recall, AVLT long-term delayed recall, and AVLT cued recall; (2) information processing speed, measured by the Symbol Digit Modalities Test, Trail Making Test Part A (TMT-A), and Stroop Color-Word Test Part A (Stroop-A); (3) executive function, assessed using the Trail Making Test Part B (TMT-B) and Stroop Color-Word Test Part C (Stroop-C); (4) language, tested with the Boston Naming Test (BNT) and Verbal Fluency Test (VFT); and (5) visuospatial function, examined using the Rey-Osterrieth Complex Figure Test (ROCF) copy task and Clock Drawing Test (CDT).

2.3. Plasma Biomarker Acquisition

Procedures for blood processing and biomarker analysis adhered to established protocols [13]. In brief, EDTA-anticoagulated venous blood was centrifuged (2000×g, 10 min, 4°C) within a 4-hour window post-collection, followed by storage at -80°C. We employed the fully automated Lumipulse G1200 system (Fujirebio, Tokyo, Japan) to determine levels of plasma p-Tau217, p-Tau181, Aβ42, Aβ40, and neurofilament light chain.

2.4. Proteomic Analysis

Large-scale proteomic profiling was executed via liquid chromatography-tandem mass spectrometry utilizing data-independent acquisition (DIA). Plasma samples were processed with the OmniProt Kit (Westlake Omics, Hangzhou, China) following manufacturer guidelines. After reduction, alkylation, and overnight trypsin digestion, peptides were desalted and fractionated on a Vanquish Neo UHPLC system (Thermo Fisher Scientific) fitted with a C18 reverse-phase column. Mass spectrometry was performed on an Orbitrap Astral unit (Thermo Fisher Scientific). DIA-NN software (v1.9) was used for raw data processing, spectral library alignment, and quantification, with protein identification filtered at a 1% false discovery rate[14].

2.5. Weighted Gene Co-expression Network Analysis

To identify protein co-expression modules associated with imaging phenotypes, WGCNA was performed using the R package "WGCNA"[15]. A scale-free co-expression network was constructed using an optimal soft-thresholding power (β) to approximate a scale-free topology. Proteins were clustered into distinct modules using a dynamic tree-cut algorithm. Module Eigengenes (MEs), representing the first principal component of each module, were calculated to summarize module expression profiles. Functional enrichment

158 analysis of key modules was conducted using Gene Ontology (GO), Reactome, and
159 Disease Ontology databases to elucidate biological functions.

160 ***2.6. MRI Acquisition and Radiomic Analysis***

161 All participants underwent 3.0 T MRI scanning on Philips Achieva and Siemens Prisma
162 systems using standardized T1-weighted imaging protocols. A common preprocessing
163 pipeline was applied across platforms, including N4 bias field correction, Z-score intensity
164 normalization, resampling to 1×1×1 mm^3 isotropic voxels, and spatial normalization to
165 Montreal Neurological Institute space using SPM12's DARTEL algorithm[16].

166 Radiomics analysis was performed on the 90 cortical and subcortical brain regions
167 defined by the Automated Anatomical Labeling (AAL) atlas using PyRadiomics v3.0.1
168 following Image Biomarker Standardisation Initiative standards[17, 18]. For each region,
169 comprehensive radiomic features were extracted across seven image types (original and
170 six mathematical transformations), capturing morphological, first-order statistical, and five
171 textural feature classes.

172 Feature selection employed a hierarchical two-stage approach. In the first stage, for
173 each of the 90 brain regions, a three-tier selection method was applied: (1) Spearman
174 correlation analysis to remove redundant features ($|r| > 0.9$), (2) Random Forest-based
175 Recursive Feature Elimination to identify the top ten most informative features, and (3)

Least Absolute Shrinkage and Selection Operator (LASSO) regression with 10-fold cross-validation for final feature refinement. In the second stage, the selected features from all brain regions were aggregated into a combined feature set, which then underwent the same three-tier selection procedure to identify the optimal feature subset. RadScore was subsequently calculated using the final selected features weighted by their LASSO coefficients, yielding an exploratory quantitative imaging score **(details in Supplementary Methods)**.

2.7. Machine Learning Modeling and Interpretability

We developed machine learning classification models using six algorithms: Support Vector Machine (SVM), Logistic Regression (LR), Random Forest (RF), Light Gradient Boosting Machine (LGB), Gaussian Naive Bayes (GNB), and Extreme Gradient Boosting (XGBoost). The cohort was stratified into a training set (70%) and a held-out internal test subset (30%). The models were trained on the training set using the radiomic features ultimately selected through our feature selection process, and their performance was evaluated on the independent test set using multiple metrics, including Area Under the Receiver Operating Characteristic Curve (AUC), accuracy, and sensitivity. To interpret the predictions, we employed Shapley Additive Explanations (SHAP). This game theory-based methodology quantifies individual feature contributions by computing SHAP values,

where the magnitude indicates the strength of influence and the sign denotes the direction of impact (promoting or suppressing the outcome).

2.8. Statistical Analysis

Statistical analyses were performed using Python (version 3.7.15) and R (version 4.4.1). Group comparisons between LLD Aβ+ and LLD Aβ- individuals utilized statistical tests selected based on data characteristics and distribution patterns. The chi-square (χ^2) test was employed for categorical variables, whereas continuous variables were analyzed using independent samples t-test for normally distributed data or Mann–Whitney U test for non-normally distributed data. All statistical tests were two-tailed, and statistical significance was defined as $p < 0.05$. To examine associations between radiomic features, RadScore, and clinical measures (including neuropsychological test scores and plasma biomarkers), partial correlation analyses were conducted adjusting for age, sex, and years of education. Additionally, exploratory cross-sectional indirect-effect analyses were performed to assess statistical compatibility with indirect pathways. In these models, protein module eigengenes served as the independent variable (X), RadScore served as the mediator (M), and cognitive domain scores (e.g., Cued Recall) served as the dependent variable (Y). All models included age, sex, and years of education as covariates.

3. Results

3.1 Demographic, clinical, and biological characteristics

The demographic and clinical characteristics of the study population are summarized in Table 1. Based on the 2024 NIA-AA revised criteria, LLD patients were stratified into amyloid-positive (LLD Aβ+) (n = 40) and amyloid-negative (LLD Aβ-) (n = 76) groups. The groups did not differ significantly in sex, education, or depressive severity ($p > 0.05$), whereas the Aβ-positive group was older ($p = 0.047$). As expected, compared with the LLD Aβ- group, the LLD Aβ+ group exhibited markedly elevated plasma levels of p-Tau217, p-Tau181, and neurofilament light chain, along with reduced Aβ42 concentrations and Aβ42/40 ratios (all $p < 0.01$). Although global cognitive performance was similar between groups, the LLD Aβ+ group demonstrated significant impairments in episodic memory (AVLT short-delay, long-delay, and cued recall; all $p < 0.05$), processing speed (TMT-A; $p = 0.009$), and verbal fluency (VFT; $p = 0.034$).

3.2 Construction, validation, and interpretability of the radiomic signature

To identify neuroimaging markers of Aβ pathology, we applied LASSO regression with 10-fold cross-validation to the extracted radiomic features. The optimal regularization parameter ($\lambda = 0.0148$) yielded a parsimonious signature comprising eight features (**Figure 2A-C,** **Table S1**), which were aggregated to calculate the RadScore. We systematically

evaluated six machine learning classifiers trained on these features (Table S2). While all models demonstrated excellent discrimination in the training cohort, the XGBoost algorithm exhibited the highest discrimination in the held-out internal test subset, achieving an AUC of 0.788 (95% CI: 0.601-0.935; **Figure 2D-E**). To examine feature contributions to these predictions, we employed SHAP analysis to quantify individual feature contributions (**Figure S1**). This analysis revealed a distributed pattern of neuroanatomical vulnerability where the top predictors included texture features derived from the right paracentral lobule and left precuneus, followed by limbic regions. Specifically, lower values of first-order mean intensity in the paracentral lobule were strongly predictive of a higher probability of amyloid positivity. These model-derived feature contributions suggest that LLD Aβ+ patients exhibit distinct microstructural heterogeneity not only in emotion regulation circuits but also in regions governing sensorimotor integration and psychomotor speed, specifically the paracentral lobule.

3.3 Biological Annotation of the Radiomics-Associated Turquoise Module

To identify plasma protein co-expression patterns associated with the radiomic phenotype in LLD, we performed WGCNA on plasma proteomics. The analysis identified five distinct co-expression modules: Black (n = 264), Turquoise (n = 87), Brown (n = 68), Pink (n = 41), and Grey (n = 41). Correlation analysis revealed that the Turquoise module

exhibited the strongest negative association with RadScore ($r = -0.49$, $p = 2 \times 10^{-8}$; **Figure 3**), while other modules showed weaker or non-significant associations. GO analysis revealed that the Turquoise module was predominantly enriched in biological processes related to innate immune dysregulation. Notably, we observed an exceptionally high fold enrichment in pathways governing "non-canonical inflammasome complex assembly" (GO:0160075) and "neutrophil apoptotic process" (GO:0001781), suggesting a specific disruption in the turnover of myeloid cells and inflammatory signaling. In the molecular function category, "cytokine activity" (GO:0005125) was identified as a core feature. Consistent with these findings, Reactome pathway analysis highlighted a signature of acute inflammatory transduction, including "Fc epsilon receptor (FCERI) signaling" (R-HSA-2454202) and the "Interleukin-36 pathway" (R-HSA-9014826). These enrichment results indicate that the RadScore-associated module contains proteins annotated to innate immune and neutrophil-related processes; they do not establish pathway activation or suppression.

3.4 Association with Aβ pathology and cognitive function

We next examined whether RadScore derived from the model was associated with AD-related plasma biomarkers and clinical measures (**Figure 4**). Across the entire cohort, RadScore demonstrated significant positive associations with plasma p-Tau181 ($r = 0.432$,

$p < 0.001$) and p-Tau217 (r = 0.217, $p = 0.022$) after adjusting for age and sex. Clinically, elevated RadScore was associated with poorer performance in short-term delayed recall (r = −0.213, $p = 0.031$) and confrontation naming (BNT; r = −0.237, $p = 0.014$). Intriguingly, within the LLD Aβ- subgroup, RadScore remained significantly associated with executive dysfunction (Stroop-C; r = 0.376, $p = 0.007$). This association may reflect non-amyloid-related sources of T1 image heterogeneity, although their biological basis cannot be determined from the present data.

3.5 Mediation analysis results

Exploratory indirect-effect analysis was conducted to examine whether the observed associations were statistically compatible with a model linking the plasma protein module, RadScore, and cognitive outcomes. We observed that the impact of the immune-related Turquoise module on memory performance (specifically AVLT cued recall) was associated with a statistically significant indirect effect through the RadScore (**Figure 5**). Specifically, reduced expression of the Turquoise module eigengene was associated with higher RadScore (β = −1.791, $p < 0.001$), which in turn was associated with worse memory function (β = −1.849, $p < 0.05$). The indirect effect via RadScore was statistically significant (Effect = 3.312, SE = 1.633, 95% CI: [0.228, 6.689]), accounting for 52.5% of the total effect. The direct association between the protein module and memory was not

283 statistically significant (β = 2.997, p = 0.344) after adjusting for the mediator, whereas the
284 total effect remained significant (β = 6.309, p = 0.018). We also examined potential
285 mediation effects in other cognitive domains, including executive function and processing
286 speed; however, no significant indirect pathways via RadScore were observed for these
287 domains, indicating that the indirect association was observed for memory but not for the
288 other tested domains.

289 ## Discussion

290 In this study, we integrated plasma proteomics, MRI-based radiomics, and cognitive
291 assessments to examine cross-modal proteomic-radiomic-cognitive associations in Late-
292 Life Depression (LLD) patients stratified by amyloid pathology. Our analysis yielded three
293 primary findings. First, we constructed an exploratory RadScore that effectively
294 distinguished LLD patients with underlying amyloid pathology (LLD Aβ+) from those
295 without. Crucially, the influential T1-derived radiomic features were spatially concentrated
296 in the paracentral lobule and precuneus, regions critical for sensorimotor integration.
297 Second, utilizing WGCNA on plasma proteomics, we identified a specific co-expression
298 module (Turquoise). This module was enriched in innate immune activation and neutrophil
299 degranulation and was strongly associated with RadScore. Third, mediation analysis
300 revealed that the RadScore showed an exploratory statistical indirect association between
301 the plasma protein module and memory performance. Collectively, these results are

consistent with, but do not establish, a biological model in which systemic innate immune profiles are associated with T1-derived radiomic heterogeneity in vulnerable sensorimotor networks. This specifically involves neutrophil-mediated pathways and co-occurs with memory impairment in this LLD sample.

The contribution of paracentral lobule features to the radiomic signature in LLD Aβ+ patients. This spatial pattern may relate to neural systems implicated in psychomotor retardation, a core phenotypic feature of the depression-executive dysfunction syndrome that distinguishes LLD from typical amnestic AD[19]. Recent large-scale neuroimaging studies have established that psychomotor retardation in depression has been associated with disrupted functional connectivity within the sensorimotor network. This specifically involves the paracentral lobule and its thalamic projections[20-22]. While classic amyloid pathology predominantly targets the medial temporal lobe, atypical AD variants often exhibit distinct regional vulnerabilities. Notably, specific AD subtypes are characterized by prominent Tau accumulation in the primary motor cortex. This accumulation correlates with domain-specific motor-executive deficits[23, 24]. Therefore, the radiomic disintegration observed in the paracentral lobule raises the hypothesis that amyloid-positive LLD may involve a psychomotor-predominant phenotype within the AD continuum. In this subtype, the intersection of depressive pathophysiology and amyloid proteinopathy disproportionately impacts motor-executive circuits.

At the molecular level, the Turquoise module exhibited the strongest correlation with brain microstructural damage. This module was functionally enriched in innate immune activation and neutrophil degranulation. This aligns with the "neuroimmunological hypothesis" of LLD. This hypothesis posits that peripheral immune dysregulation is a pivotal shared mechanism driving both depression and neurodegeneration[25, 26]. Crucially, our findings extend beyond general systemic inflammation. Consistent with recent proteomic analysis of CSF in AD, proteins associated with cell adhesion and inflammation have been specifically linked to depressive symptoms rather than cognitive decline alone[27]. Our peripheral data identify an immune-enriched protein module in LLD, but do not establish a depression-specific signature. While amyloid pathology itself involves immune activation, the coexistence of LLD may be associated with a neutrophil-related plasma protein profile. Emerging evidence indicates that neutrophils are typically restricted from entering the CNS. However, in AD models, they can infiltrate the brain parenchyma and release neutrophil extracellular traps (NETs) that exacerbate neurotoxicity[26, 28]. Whether the Turquoise module reflects an additive or interacting process specific to LLD cannot be determined without an amyloid-positive non-LLD comparison group.

A possible biological model concerns how peripheral immune profiles might relate to the regionally specific T1-derived radiomic features captured by the RadScore. The BBB

is one plausible, but unmeasured, link in this proposed cross-modal model. Systemic inflammation is a well-documented driver of BBB endothelial dysfunction, particularly the neutrophil-derived mediators identified in our Turquoise module[29]. This barrier breakdown likely facilitates the infiltration of neurotoxic plasma factors or immune cells into the brain parenchyma. Once central, these factors can trigger a local glial response. Indeed, oligodendrocytes have been shown to actively modulate immune responses via tumor necrosis factor receptor 2 signaling. This influences BBB permeability and immune cell infiltration[30]. Our radiomic features are characterized by increased textural heterogeneity, but the present data cannot determine whether this pattern reflects microglial activation, demyelination, edema, or other tissue processes. These processes have been histologically validated to correlate with MRI texture anomalies even in normal-appearing white matter[31, 32]. Accordingly, the immune-BBB interpretation should be viewed as a hypothesis for future multimodal testing rather than as a process established by the present study.

Limitations

Several limitations should be acknowledged. First, the cross-sectional, single-center design and relatively small sample size limit causal inference and generalizability, underscoring the need for larger longitudinal and multicenter validation. Second, the lack of CSF proteomic data limited biological interpretation of the radiomic features.

Conclusions

In conclusion, our study identifies convergent cross-modal associations in LLD patients with amyloid pathology. A plasma protein module enriched for innate immune and neutrophil-related annotations was associated with a T1-derived radiomic score that included influential paracentral lobule features. This region serves as a key node for psychomotor function. The RadScore also showed an exploratory statistical indirect association with memory performance. These findings highlight biological heterogeneity within LLD and require independent, longitudinal validation before clinical or therapeutic interpretation.

List of abbreviations

AAL, Automated Anatomical Labeling;

AD, Alzheimer's disease;

APOE, apolipoprotein E;

AUC, area under the curve;

AVLT, Auditory Verbal Learning Test;

Aβ, amyloid-beta;

BBB, blood-brain barrier;

BNT, Boston Naming Test;

CDR, Clinical Dementia Rating Scale;

CDT, Clock Drawing Test;

CI, confidence interval;

CNS, central nervous system;

CSF, cerebrospinal fluid;

DARTEL, Diffeomorphic Anatomical Registration Through Exponentiated Lie Algebra;

DIA, data-independent acquisition;

DIA-NN, data-independent acquisition by neural networks;

DSM-5, Diagnostic and Statistical Manual of Mental Disorders, Fifth Edition;

EDTA, ethylenediaminetetraacetic acid;

FCERI, Fc epsilon receptor I;

GNB, Gaussian Naive Bayes;

GO, Gene Ontology;

HAMD-17, 17-item Hamilton Depression Rating Scale;

LASSO, Least Absolute Shrinkage and Selection Operator;

LGB, Light Gradient Boosting Machine;

LLD, late-life depression;

LR, Logistic Regression;

ME, module eigengene;

MMSE, Mini-Mental State Examination;

MRI, magnetic resonance imaging;

MSE, mean squared error;

NETs, neutrophil extracellular traps;

NfL, neurofilament light chain;

NIA-AA, National Institute on Aging–Alzheimer's Association;

PET, positron emission tomography;

p-Tau181, tau phosphorylated at threonine 181;

p-Tau217, tau phosphorylated at threonine 217;

RadScore, radiomics score;

RF, Random Forest;

ROC, receiver operating characteristic;

ROCF, Rey–Osterrieth Complex Figure Test;

SDMT, Symbol Digit Modalities Test;

SE, standard error;

SHAP, Shapley Additive Explanations;

SPM12, Statistical Parametric Mapping 12;

Stroop-A, Stroop Color-Word Test Part A;

Stroop-C, Stroop Color-Word Test Part C;

SVM, Support Vector Machine;

TMT-A, Trail Making Test Part A;

TMT-B, Trail Making Test Part B;

UHPLC, ultra-high-performance liquid chromatography;

VFT, Verbal Fluency Test;

WGCNA, weighted gene co-expression network analysis;

XGBoost, Extreme Gradient Boosting.

References

[1] Livingston G, Huntley J, Sommerlad A, Ames D, Ballard C, Banerjee S, et al. Dementia prevention, intervention, and care: 2020 report of the Lancet Commission. Lancet. 2020;396:413–46.

[2] Elser H, Horváth-Puhó E, Gradus JL, Smith ML, Lash TL, Glymour MM, et al. Association of Early-, Middle-, and Late-Life Depression With Incident Dementia in a Danish Cohort. JAMA Neurol. 2023;80:949–58.

[3] Jellinger KA. The heterogeneity of late-life depression and its pathobiology: a brain network dysfunction disorder. J Neural Transm (Vienna). 2023;130:1057–76.

[4] Alexopoulos GS. Mechanisms and treatment of late-life depression. Transl Psychiatry. 2019;9:188.

[5] Song J, Ma Z, Zhang H, Liang T, Zhang J. Identification of novel biomarkers linking depressive disorder and Alzheimer's disease based on an integrative bioinformatics analysis. BMC Genom Data. 2023;24:22.

[6] Diniz BS, Lin CW, Sibille E, Tseng G, Lotrich F, Aizenstein HJ, et al. Circulating biosignatures of late-life depression (LLD): Towards a comprehensive, data-driven approach to understanding LLD pathophysiology. J Psychiatr Res. 2016;82:1–7.

[7] Smagula SF, Lotrich FE, Aizenstein HJ, Diniz BS, Krystek J, Wu GF, et al. Immunological biomarkers associated with brain structure and executive function in late-life depression: exploratory pilot study. Int J Geriatr Psychiatry. 2017;32:692–9.

[8] Duggan MR, Yang Z, Cui Y, Dark HE, Wen J, Erus G, et al. Proteomic analyses reveal plasma EFEMP1 and CXCL12 as biomarkers and determinants of neurodegeneration. Alzheimers Dement. 2024;20:6486–505.

[9] Cheung EYW, Chau ACM, Tang FH, On Behalf Of The Alzheimer's Disease Neuroimaging I. Radiomics-Based Artificial Intelligence Differentiation of Neurodegenerative Diseases with Reference to the Volumetry. Life (Basel). 2022;12:514.

[10] Lambin P, Rios-Velazquez E, Leijenaar R, Carvalho S, van Stiphout RG, Granton P, et al. Radiomics: extracting more information from medical images using advanced feature analysis. Eur J Cancer. 2012;48:441–6.

[11] Lee S, Lee H, Kim KW. Magnetic resonance imaging texture predicts progression to dementia due to Alzheimer disease earlier than hippocampal volume. J Psychiatry Neurosci. 2020;45:7–14.

[12] Jack CR, Jr., Andrews JS, Beach TG, Buracchio T, Dunn B, Graf A, et al. Revised criteria for diagnosis and staging of Alzheimer's disease: Alzheimer's Association Workgroup. Alzheimers Dement. 2024;20:5143–69.

[13] Zhong X, Wang Q, Yang M, Lin G, Yao K, Wu Z, et al. Plasma p-tau217 and p-tau217/Aβ1-42 are effective biomarkers for identifying CSF- and PET imaging-

diagnosed Alzheimer's disease: Insights for research and clinical practice. Alzheimers Dement. 2025;21:e14536.
[14] Demichev V, Messner CB, Vernardis SI, Lilley KS, Ralser M. DIA-NN: neural networks and interference correction enable deep proteome coverage in high throughput. Nat Methods. 2020;17:41–4.
[15] Langfelder P, Horvath S. WGCNA: an R package for weighted correlation network analysis. BMC Bioinformatics. 2008;9:559.
[16] Ashburner J. A fast diffeomorphic image registration algorithm. Neuroimage. 2007;38:95–113.
[17] Rolls ET, Joliot M, Tzourio-Mazoyer N. Implementation of a new parcellation of the orbitofrontal cortex in the automated anatomical labeling atlas. Neuroimage. 2015;122:1–5.
[18] van Griethuysen JJM, Fedorov A, Parmar C, Hosny A, Aucoin N, Narayan V, et al. Computational Radiomics System to Decode the Radiographic Phenotype. Cancer Res. 2017;77:e104–e7.
[19] Alexopoulos GS, Kiosses DN, Klimstra S, Kalayam B, Bruce ML. Clinical presentation of the "depression-executive dysfunction syndrome" of late life. Am J Geriatr Psychiatry. 2002;10:98–106.
[20] Song XM, Liu DY, Hirjak D, Hu XW, Han JF, Roe AW, et al. Motor versus Psychomotor? Deciphering the Neural Source of Psychomotor Retardation in Depression. Adv Sci (Weinh). 2024;11:e2403063.
[21] Wüthrich F, Lefebvre S, Mittal VA, Shankman SA, Alexander N, Brosch K, et al. The neural signature of psychomotor disturbance in depression. Mol Psychiatry. 2024;29:317–26.
[22] Su T, Chen B, Yang M, Wang Q, Zhou H, Zhang M, et al. Disrupted functional connectivity of the habenula links psychomotor retardation and deficit of verbal fluency and working memory in late-life depression. CNS Neurosci Ther. 2024;30:e14490.
[23] Petersen C, Nolan AL, de Paula França Resende E, Miller Z, Ehrenberg AJ, Gorno-Tempini ML, et al. Alzheimer's disease clinical variants show distinct regional patterns of neurofibrillary tangle accumulation. Acta Neuropathol. 2019;138:597–612.
[24] Ossenkoppele R, Cohn-Sheehy BI, La Joie R, Vogel JW, Möller C, Lehmann M, et al. Atrophy patterns in early clinical stages across distinct phenotypes of Alzheimer's disease. Hum Brain Mapp. 2015;36:4421–37.
[25] Huang YY, Gan YH, Yang L, Cheng W, Yu JT. Depression in Alzheimer's Disease: Epidemiology, Mechanisms, and Treatment. Biol Psychiatry. 2024;95:992–1005.
[26] Jorfi M, Maaser-Hecker A, Tanzi RE. The neuroimmune axis of Alzheimer's disease. Genome Med. 2023;15:6.

[27] Rabl M, Hartog WL, van der Flier WM, Pijnenburg YAL, Teunissen CE, Tsolaki M, et al. Cerebrospinal fluid proteome alterations related to depressive symptoms in cognitive decline and Alzheimer's disease. Alzheimers Dement. 2025;21:e71054.
[28] Smyth LCD, Murray HC, Hill M, van Leeuwen E, Highet B, Magon NJ, et al. Neutrophil-vascular interactions drive myeloperoxidase accumulation in the brain in Alzheimer's disease. Acta Neuropathol Commun. 2022;10:38.
[29] Sweeney MD, Sagare AP, Zlokovic BV. Blood-brain barrier breakdown in Alzheimer disease and other neurodegenerative disorders. Nat Rev Neurol. 2018;14:133–50.
[30] Madsen PM, Desu HL, de Rivero Vaccari JP, Florimon Y, Ellman DG, Keane RW, et al. Oligodendrocytes modulate the immune-inflammatory response in EAE via TNFR2 signaling. Brain Behav Immun. 2020;84:132–46.
[31] Cai JH, He Y, Zhong XL, Lei H, Wang F, Luo GH, et al. Magnetic Resonance Texture Analysis in Alzheimer's disease. Acad Radiol. 2020;27:1774–83.
[32] Tozer DJ, Zeestraten E, Lawrence AJ, Barrick TR, Markus HS. Texture Analysis of T1-Weighted and Fluid-Attenuated Inversion Recovery Images Detects Abnormalities That Correlate With Cognitive Decline in Small Vessel Disease. Stroke. 2018;49:1656–61.

Declarations

Ethics approval and consent to participate

All participants or their legal guardians provided signed informed consent to participate in the study. The study was conducted in accordance with the Declaration of Helsinki and was approved by the Ethics Committee of the Affiliated Brain Hospital of Guangzhou Medical University (Approval No. AF/SC-02/02.1).

Consent for publication

Not applicable.

Availability of data and materials

The data that support the findings of this study are available from the corresponding author upon reasonable request.

Conflicts of Interest

The authors declare that they have no conflicts of interests.

Funding

The study was supported by Guangdong Province Key Areas Research and Development Programs-Brain Science and Brain-Inspired Intelligence Technology (2023B0303010003), National Traditional Chinese and Western Medicine Collaborative Project for Major and Complex Diseases (Comprehensive Department of the National Administration of Traditional Chinese Medicine [2024] No. 3), National Integrated Traditional Chinese and Western Medicine "Flagship" Department Construction Project (Comprehensive Department of the National Administration of Traditional Chinese Medicine [2024] No. 221), Guangzhou Clinical Advanced, Major and Distinctive

Technology Project (2026–2028), Guangzhou Second Batch Major and Difficult (Rare) Diseases Diagnosis and Treatment Center Project (2026ZLZX-20), Guangdong Provincial Key Clinical Specialty Construction Project (Geriatrics Department) and Southern China Young Physicians Clinical Collaboration Program in Neuropsychiatry (2025GDMHA00).

Authors' contributions

Danyan Xu, Pengbo Gao, and Weilin Wang contributed equally to data analysis, image processing, data interpretation, and manuscript writing. Huanmin Liu, Wei He, Ting Su, and Youxuan Zheng participated in image processing and statistical analysis. Zhen Peng, Haoye Tan, Mingfeng Yang, Qiang Wang, Zhidai Xiao were primarily responsible for data collection. Ben Chen, Xiaomei Zhong, and Yuping Ning provided the theoretical framework for this work, designed the experimental approach, supervised the study, and provided critical review and suggestions. All authors have read and approved the final manuscript.

Acknowledgments

We express our deepest gratitude to all participants and their families for their invaluable contributions to this study. We extend our sincere appreciation to the clinical and research staff at the Affiliated Brain Hospital of Guangzhou Medical University for their dedicated support and expertise throughout the conduct of this work.

Figure Legend

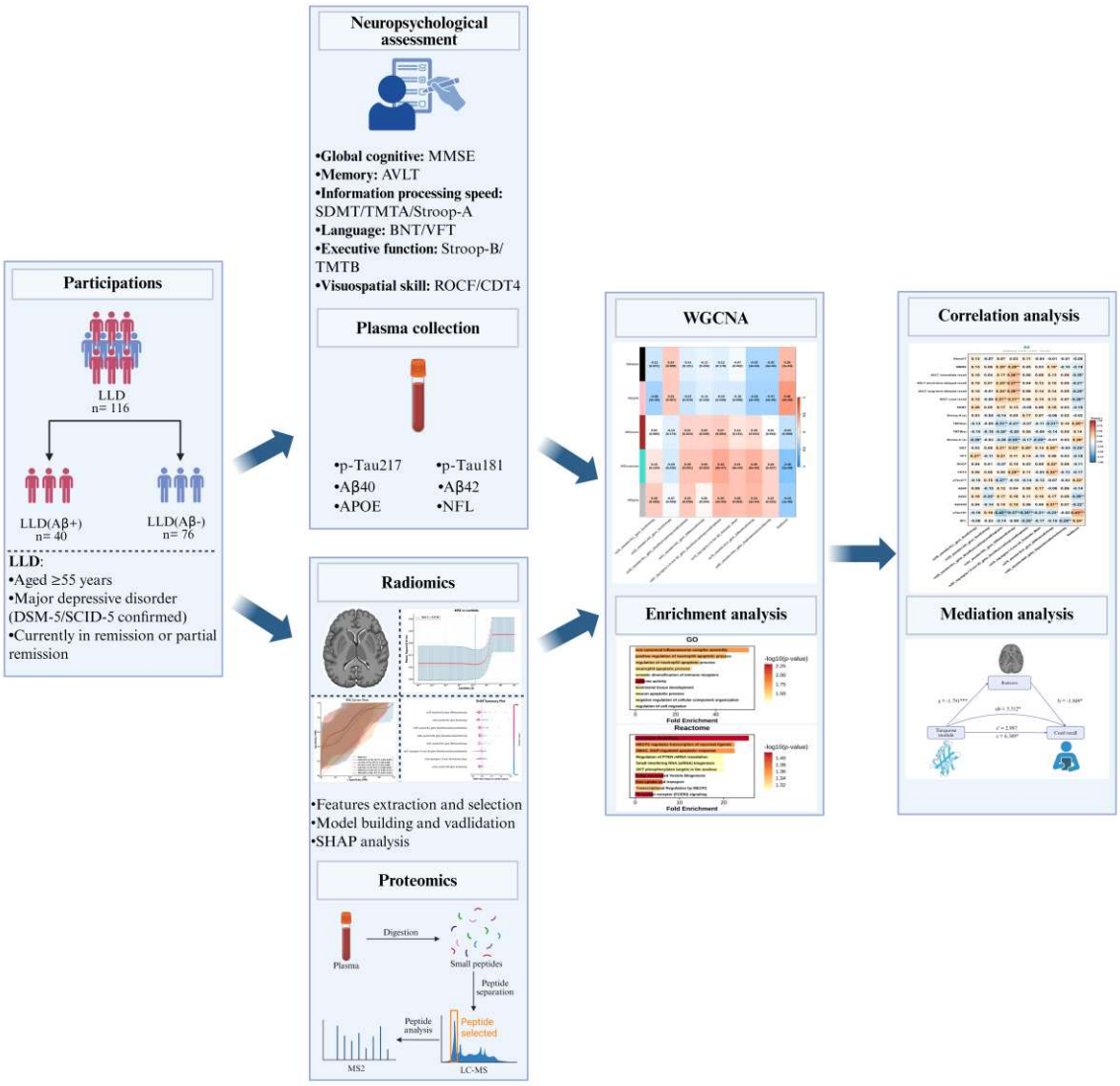


Figure 1. Study design and analytical workflow. The schematic illustrates the dual-omics framework comprising three phases: (1) Hierarchical Biomarker-Based Classification: A total of 116 patients with Late-Life Depression (LLD) were consecutively enrolled and stratified into amyloid-positive (LLD Aβ+, n=40) and amyloid-negative (LLD Aβ-, n=76) groups. (2) Multi-modal Phenotyping: Data acquisition involved: (i) a standardized neuropsychological battery covering five cognitive domains (memory, executive function, speed, language, visuospatial); (ii) high-resolution T1-weighted MRI for radiomic feature extraction; and (iii) large-scale plasma proteomic profiling utilizing

Data-Independent Acquisition (DIA) mass spectrometry to ensure deep proteome coverage. (3) Cross-Modal Association: The analytical pipeline integrated machine learning-based radiomics (to construct RadScore), Weighted Gene Co-expression Network Analysis (WGCNA) (to identify immune-specific protein modules), and exploratory cross-sectional indirect-effect modeling to assess whether the observed protein–radiomic–cognitive associations were compatible with the prespecified "Immune-Brain-Cognition" framework. Abbreviations: AD, Alzheimer's disease; Aβ, amyloid-beta; DIA, data-independent acquisition; LLD, late-life depression; MRI, magnetic resonance imaging; PET, positron emission tomography; WGCNA, weighted gene co-expression network analysis.

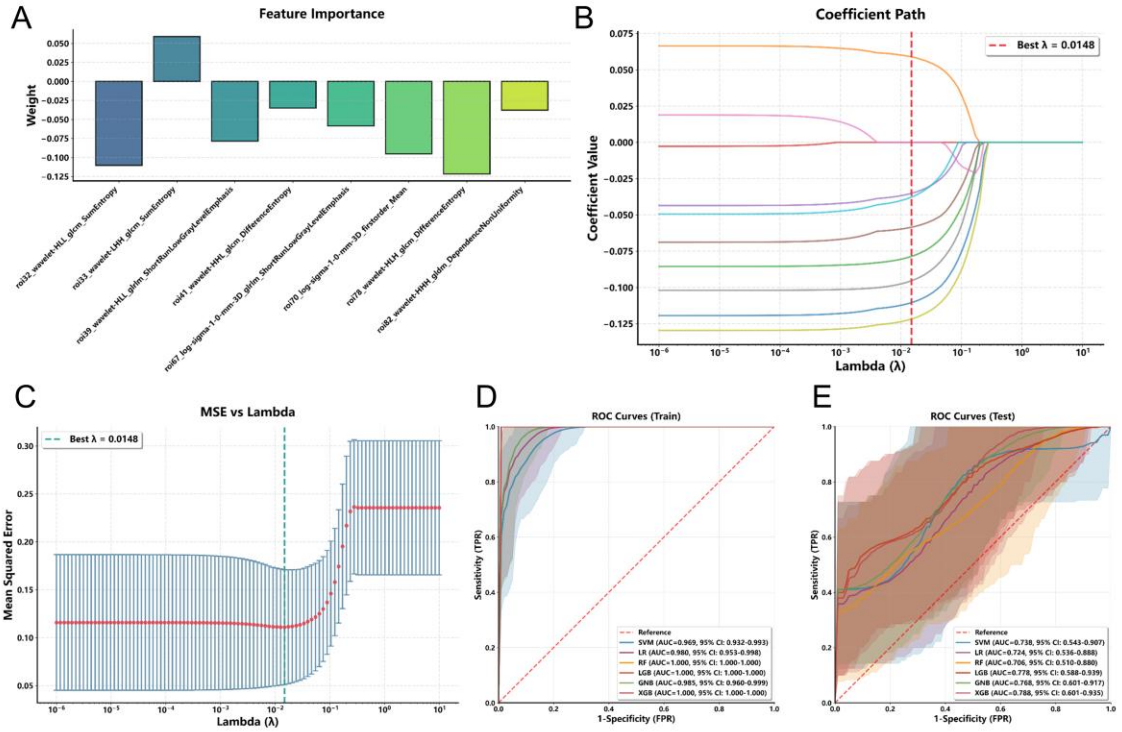


Figure 2. Radiomic signature construction for amyloid pathology classification. (A) Least Absolute Shrinkage and Selection Operator (LASSO) regression identified eight radiomic features, displayed weighted by their respective coefficients. (B) Cross-validation coefficient paths of the radiomic features. (C) Mean Squared Error (MSE) versus log(λ) with 10-fold cross-validation error bars. The vertical dashed line indicates the optimal λ value (0.0148) that minimized the prediction error. (D, E) Receiver Operating

Characteristic (ROC) curves comparing the discriminative performance of six machine learning classifiers (SVM, LR, RF, LGB, GNB, and XGBoost) in distinguishing LLD Aβ+ from LLD Aβ- patients in the training set (D) and the held-out internal test subset (E). The XGBoost model (red line) achieved the highest discrimination in this internal subset, achieving the highest Area Under the Curve (AUC) of 0.788 (95% CI: 0.601 – 0.935), supporting further evaluation in independent cohorts. Abbreviations: AD, Alzheimer's disease; Aβ, amyloid-beta; AUC, area under the curve; CI, confidence interval; GNB, Gaussian Naive Bayes; LASSO, least absolute shrinkage and selection operator; LGB, light gradient boosting machine; LLD, late-life depression; LR, logistic regression; MSE, mean squared error; RF, random forest; ROC, receiver operating characteristic; SVM, support vector machine; XGBoost, extreme gradient boosting.

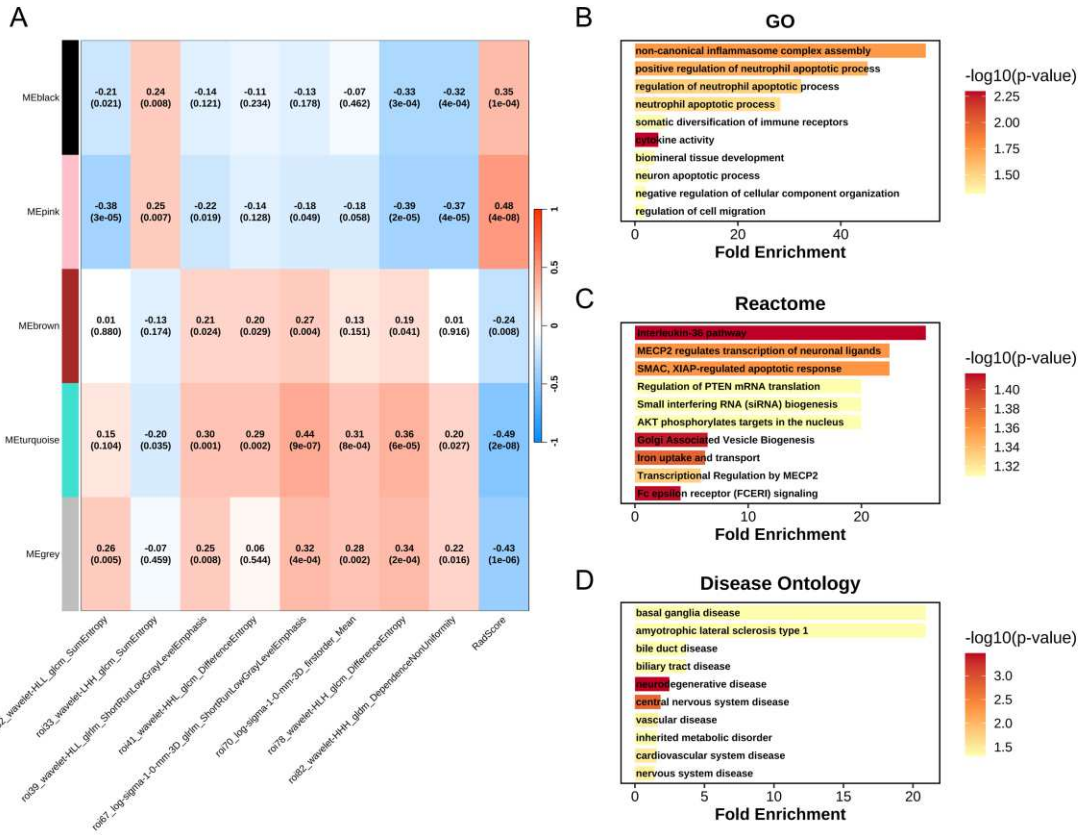


Figure 3. Proteomic identification of the RadScore-associated protein co-expression module. (A) Module-Trait Correlation: Heatmap displaying the correlation matrix between proteomic module eigengenes (rows) and radiomic features (columns), quantified

via Pearson correlation analysis. Notably, the Turquoise module exhibited the most robust negative association with RadScore ($r = -0.49$, $p < 0.001$), identifying it as the protein module most strongly associated with the radiomic phenotype. (B–D) Functional Annotation of the Turquoise Module: Enrichment analyses revealing the biological roles of proteins within this key module. (B) Gene Ontology (GO) Biological Processes: The top enriched terms cluster around innate immune dysregulation, specifically "non-canonical inflammasome complex assembly" and "neutrophil apoptotic process," suggesting a specific disruption in myeloid cell turnover and inflammatory signaling. (C) Reactome Pathways: Consistent with the GO findings, pathway analysis highlights active immune signaling and apoptosis-related regulation. (D) Disease Ontology: The module proteins are preferentially mapped to neurodegenerative diseases and central nervous system disorders, indicating annotation overlap with neurodegenerative and central nervous system disorders.
Abbreviations: GO, Gene Ontology; RadScore, radiomics score.

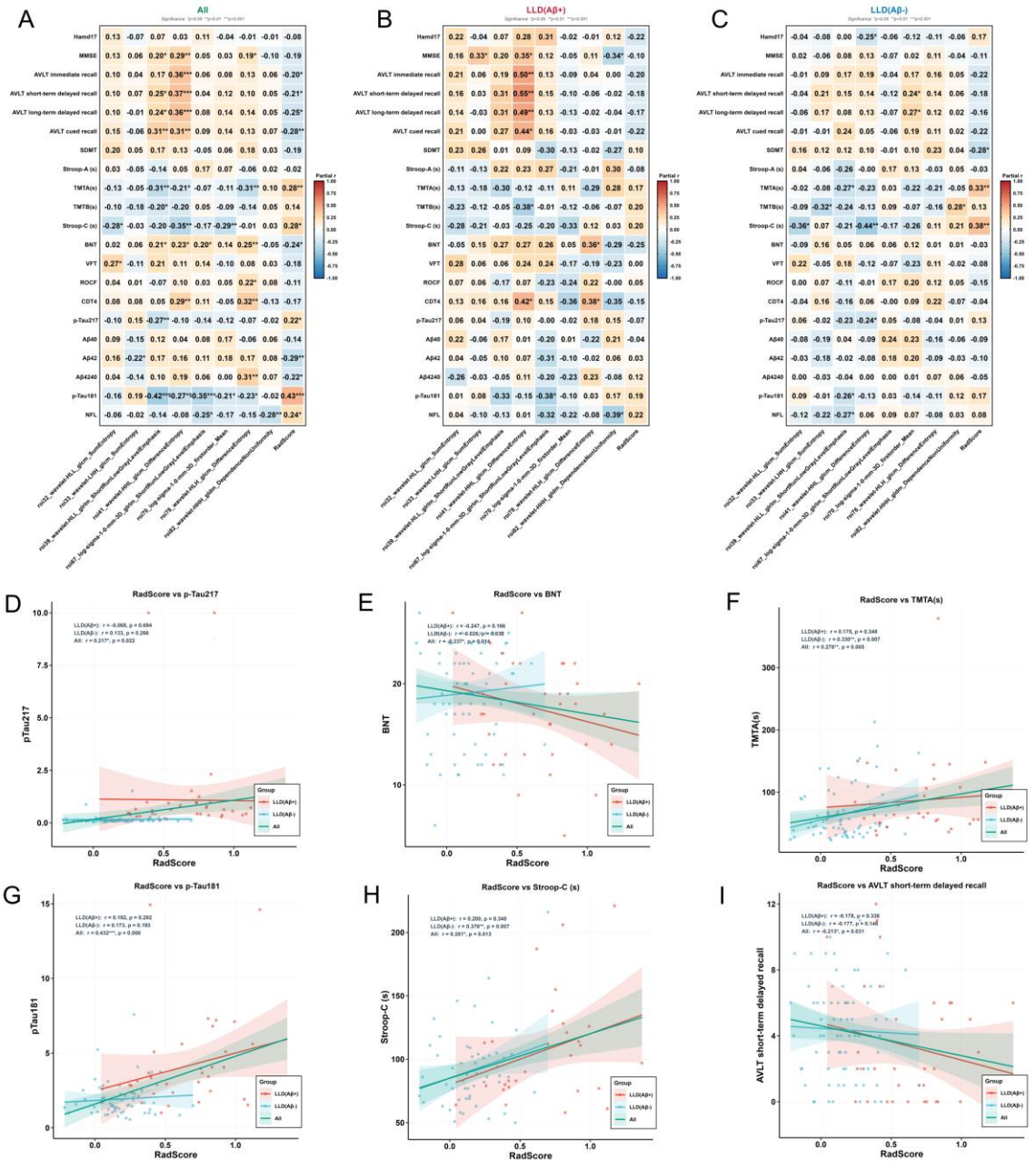


Figure 4. Associations of RadScore with AD-related plasma biomarkers and cognition. (A–C) Partial correlation heatmaps displaying the associations between individual radiomic features, RadScore, and clinical measures after adjusting for age, sex, and education. The analyses are stratified into: (A) the full cohort, (B) the LLD Aβ+ subgroup, and (C) the LLD Aβ- subgroup. The color intensity represents the correlation strength (*p < 0.05, **p < 0.01, ***p < 0.001). (D–I) Scatterplots illustrating the specific correlations between RadScore and key biological/cognitive markers: (D, G) Biological Validation:

RadScore showed significant positive correlations with plasma neurodegenerative biomarkers p-Tau181 (D, r = 0.432) and p-Tau217 (G, r = 0.217), showing convergent associations between RadScore and AD-related plasma biomarkers. (E, F, H, I) Clinical Relevance: Higher RadScore was significantly associated with comprehensive cognitive decline, including poorer performance in Language (BNT, E), Processing Speed (TMT-A, F), Executive Function (Stroop-C, H), and Episodic Memory (AVLT short-delay recall, I). Note that for TMT-A and Stroop-C, positive correlations indicate longer completion times (worse performance), whereas for BNT and AVLT, negative correlations indicate lower scores (worse performance). **Abbreviations:** AD, Alzheimer's disease; AVLT, Auditory Verbal Learning Test; BNT, Boston Naming Test; LLD, late-life depression; p-Tau, phosphorylated Tau; RadScore, radiomics score; Stroop-C, Stroop Color-Word Test Part C; TMT-A, Trail Making Test Part A.

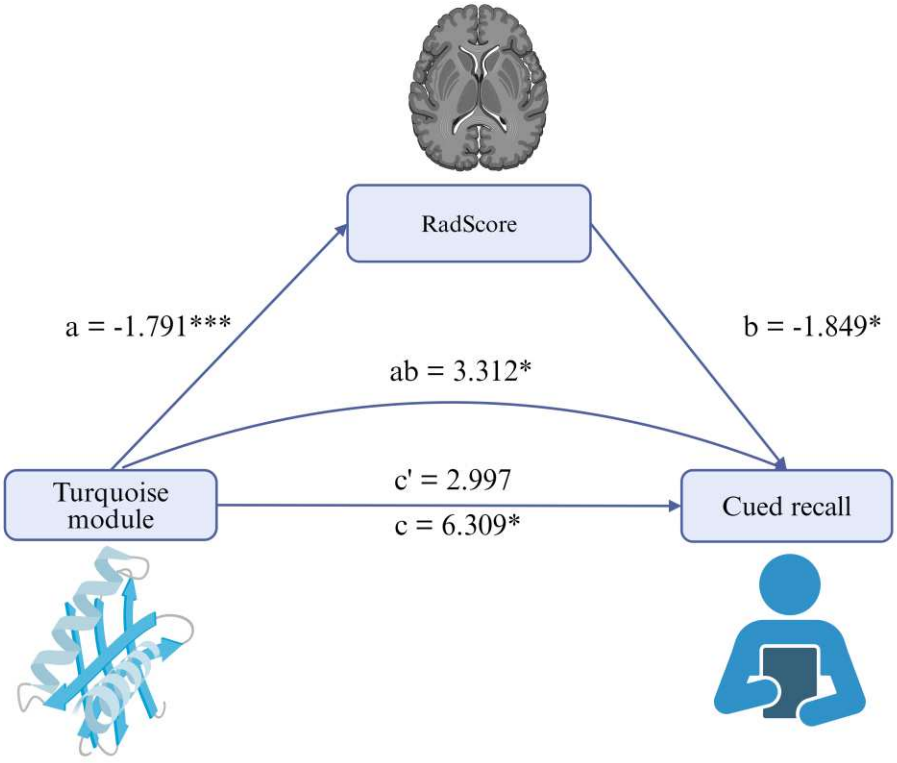


Figure 5. Exploratory indirect-effect model linking the protein module, RadScore, and memory. The path diagram summarizes an exploratory cross-sectional indirect-effect

model assessing whether RadScore statistically accounts for part of the association between the plasma protein module and cued recall. The Turquoise protein module (enriched for innate-immune and neutrophil-related annotations) was entered as the predictor (X), RadScore as the intervening statistical variable (M), and cued recall performance as the outcome (Y). Analyses were adjusted for age, sex, and education. Numbers on the arrows indicate standardized regression coefficients (β) and their corresponding *p*-values. The model showed a negative association between the Turquoise module and RadScore (Path a), while RadScore was positively associated with cued recall (Path b). The statistically significant indirect effect indicates that the observed associations were compatible with the specified statistical model; the cross-sectional design does not establish temporal direction or a causal mechanism.

668 **Table 1. Demographic, Clinical Characteristics, and Plasma Biomarkers in LLD**
669 **Patients**

	LLD (Aβ+) (N=40)	LLD (Aβ-) (N=76)	*p value*
Sex (male %)	8 (20.0%)	20 (26.3%)	0.598 [c]
Age (years)	70.83 (7.72)	68.21 (6.06)	**0.047** [b]
Education (years)	8.92 (3.57)	9.27 (4.22)	0.797 [a]
HAMD-17	10.28 (7.92)	12.91 (8.00)	0.105 [a]
APOE ε4 (carrier%)	22 (55.0%)	29 (38.2%)	0.124 [c]
Plasma biomarkers			
p-Tau217 (pg/mL)	1.10 (2.14)	0.16 (0.19)	**<0.001** [a]
Aβ40 (pg/mL)	263.66 (62.21)	275.46 (55.20)	0.135 [a]
Aβ42 (pg/mL)	22.11 (6.47)	27.26 (6.26)	**<0.001** [b]
Aβ42/40	0.08 (0.02)	0.10 (0.02)	**<0.001** [a]
NfL (pg/mL)	123.21 (436.14)	22.33 (17.38)	**0.002** [a]
p-Tau181 (pg/mL)	4.14 (3.18)	1.92 (1.19)	**<0.001** [a]
Global cognitive function			
MMSE	19.85 (6.42)	21.68 (5.74)	0.131 [a]
CDR	0.72 (0.46)	0.64 (0.45)	0.151 [a]
Memory			
AVLT immediate recall	13.51 (7.62)	14.60 (6.27)	0.158 [a]
AVLT short-term delayed recall	3.34 (3.58)	4.36 (2.85)	**0.046** [a]
AVLT long-term delayed recall	2.56 (3.57)	3.93 (2.89)	**0.005** [a]
AVLT cued recall	2.25 (3.56)	3.60 (3.11)	**0.005** [a]
Information processing speed			
SDMT (s)	21.38 (12.67)	26.40 (15.60)	0.138 [b]
Stroop A (s)	34.13 (9.25)	32.75 (13.49)	0.130 [a]
TMT A	86.57 (63.01)	64.84 (41.34)	**0.009** [a]
Executive function			

	LLD (Aβ+) (N=40)	LLD (Aβ-) (N=76)	*p value*
TMT B	99.52 (50.71)	91.95 (60.73)	0.257 [a]
Stroop C (s)	107.64 (42.44)	91.80 (30.34)	0.102 [a]
Language			
BNT	17.51 (5.11)	19.10 (4.68)	0.097 [a]
VFT	10.89 (4.78)	13.09 (4.14)	**0.034** [b]
Visuospatial			
ROCF	19.38 (10.61)	21.71 (8.68)	0.352 [a]
CDT4	2.78 (1.10)	3.15 (0.93)	0.123 [a]

Abbreviations: LLD, Late-Life Depression; p-Tau, phosphorylated Tau; Aβ, amyloid-β; APOE, apolipoprotein E; AVLT, Auditory Verbal Learning Test; BNT, Boston Naming Test; CDR, Clinical Dementia Rating; CDT, Clock Drawing Test (4-point); HAMD-17, 17-item Hamilton Depression Rating Scale; MMSE, Mini-Mental State Examination; NfL, neurofilament light chain; ROCF, Rey–Osterrieth Complex Figure Test; SDMT, Symbol Digit Modalities Test; Stroop A/C, Stroop Color and Word Test Part A/C; TMT A/B, Trail Making Test Part A/B; VFT, Verbal Fluency Test. Continuous variables are reported as mean ± standard deviation. [a] Mann-Whitney Test; [b] Two-sample *t*-test; [c] chi-square test.

Table S1. Radiomics features selected for RadScore model construction using LASSO method.

index	Feature Name	Weighted.
0	(Intercept)	0.345679
1	roi32_wavelet-HLL_glcm_SumEntropy	-0.110472
2	roi33_wavelet-LHH_glcm_SumEntropy	0.058917
3	roi39_wavelet-HLL_glrlm_ShortRunLowGrayLevelEmphasis	-0.078638
4	roi41_wavelet-HHL_glcm_DifferenceEntropy	-0.035188
5	roi67_log-sigma-1-0-mm-3D_glrlm_ShortRunLowGrayLevelEmphasis	-0.058523
6	roi70_log-sigma-1-0-mm-3D_firstorder_Mean	-0.095408
7	roi78_wavelet-HLH_glcm_DifferenceEntropy	-0.121743
8	roi82_wavelet-HHH_gldm_DependenceNonUniformity	-0.037801

Table S2. Performance comparison of different machine learning algorithms in classification tasks.

		SVM	LR	RF	LGB	GNB	XGB
Train	AUC	0.968	0.981	1.000	1.000	0.985	1.000
	Accuracy	0.889	0.926	0.988	1.000	0.938	1.000
	Sensitivity	0.786	0.857	1.000	1.000	0.857	1.000
	Specificity	0.943	0.962	0.981	1.000	0.981	1.000
	F1 Score	0.830	0.889	0.983	1.000	0.906	1.000
Test	AUC	0.739	0.728	0.710	0.779	0.772	0.790
	Accuracy	0.714	0.714	0.686	0.771	0.743	0.800
	Sensitivity	0.417	0.417	0.417	0.583	0.417	0.583
	Specificity	0.870	0.870	0.826	0.870	0.913	0.913
	F1 Score	0.500	0.500	0.476	0.636	0.526	0.667

Abbreviations: SVM, Support Vector Machine; LR, Logistic Regression; RF, Random Forest; LGB, LightGBM; GNB, Gaussian Naive Bayes; XGB, XGBoost; AUC, Area Under the Curve;

Supplementary Files

This is a list of supplementary files associated with this preprint. Click to download.

- Supplementarymaterial.docx